

Electron dynamics in strong laser pulse illumination of large rare gas clusters

Ulf Saalmann and Jan M. Rost

Max Planck Institute for the Physics of Complex Systems, Nöthnitzer Str. 38, 01187 Dresden, Germany

Received: date / Revised version: date

Abstract. We analyze the dynamics of up to 10^5 electrons resulting from illuminating a Xenon cluster with 9093 atoms with intense laser pulses of different length and peak intensity. Interesting details of electron motion are identified which can be probed with a time resolution of 100 attoseconds. Corresponding experiments would shed light on unexplored territory in complex electronic systems such as clusters and they would also permit to critically access the present theoretical description of this dynamics.

PACS. 36.40.Gk Plasma and collective effects in clusters – 31.15.Qg Molecular dynamics and other numerical methods – 36.40.Wa Charged clusters – 33.80.Wz Other multiphoton processes

1 Introduction

Recent advance in laser technology has led to the creation of subfemtosecond (100 attosecond) strong laser pulses which allow one in the future to resolve much shorter time scales in microscopic dynamics [1,2] than it has been possible so far. More specifically, while until now vibrational motion in molecules could be resolved in time experimentally, it will be possible to follow electronic motion with attosecond resolution. Still, the atomic time unit, i.e., the period of the ground state electron in hydrogen, is of the order of 10^{-17} s, i.e., roughly 10 attoseconds while for now a pulse length of 100 attoseconds and more is experimentally feasible. However, there are alternative methods such as tomographic imaging which use the high harmonic spectrum of a femtosecond pulse to get attosecond resolved dynamics. In this way it could be demonstrated that the *electronic* wavefunction of a molecule could be directly imaged [3]. This is fantastic progress, yet one might argue that we know in principle the electronic wavefunction of a diatomic molecule. We can even calculate it, and as it turns out experimental imaging and theoretical calculations via a standard solution of the Schrödinger equation agree well [3].

On the other hand, for systems more complex than a diatomic molecule, e.g., a cluster consisting of many atoms, we neither know with certainty theoretically the dynamics of the electrons (we have to make model assumptions) nor do we have a way so far to access the electron dynamics time resolved in the experiment.

Pioneering experiments [4] have demonstrated non-trivial time dependent dynamics in cluster motion under a strong laser pulse. This interesting dynamics can be attributed to resonance like behavior where either the next neighbor ions contribute in a cooperative way to enhance

ionization [5] or the electrons, still bound to the cluster but not to individual atoms, enter a collective phase of motion which is susceptible to resonant absorption of radiation [6]. Besides that, a nonlinear excitation of this resonance could be relevant [7]. A slightly different situation results from irradiation with VUV pulses as realized with the free electron laser [8]. There, inverse Bremsstrahlung seems to be the main mechanism of energy absorption. Details, however, remain controversial [9,10]. Detailed knowledge would require the experimental ability to time resolve the electron motion. Since the electrons are no longer strongly bound to a single ion but to the extended cluster, there typical time scale of motion is a bit slower which would be ideal for probing it with subfemtosecond laser light.

It is the purpose of this paper to explore which kind of details the electron dynamics exhibits during a standard femtosecond laser pulse a length of the order of 100 fs. Specifically, we will concentrate on energy spectra of electrons from a Xenon cluster with 9093 atoms during the irradiation with a laser pulse of length from 25 to 400 fs and peak intensity ranging from 10^{14} to 10^{16} W/cm².

2 Theoretical method

Before we start to discuss the spectra we give a brief account of the theoretical method how these spectra have been obtained. The initial cluster configuration is derived assuming an icosahedral symmetry of the atoms. The faces of the n th shell contain $(n+1)(n+2)/2$ atoms. Keeping only those atoms which are inside a sphere of radius $R_0 = 50$ Å yields a cluster with 9093 atoms. This configuration is relaxed using pairwise Lennard-Jones potentials to find the optimum interatomic distances thereby freezing the cluster geometry.

The laser pulse has the form of a Gaussian (we use atomic units if not stated otherwise)

$$\begin{aligned} \mathbf{F}(t) &= \hat{\mathbf{z}} F_t \cos \omega t \\ &= \hat{\mathbf{z}} \sqrt{I} \exp \left[\log 2 (2t/T)^2 \right] \cos \omega t \end{aligned} \quad (1)$$

with half width T which measures the pulse length, peak intensity I and the laser frequency of $\omega = 0.058$ a.u. (corresponding to 780 nm wavelength). The light is linearly polarized along the z -axis, denoted by the unit vector $\hat{\mathbf{z}}$. To make the simulation tractable we only model explicitly the outermost bound electron of an atom/ion [6]. In this way more and more electrons “are generated” due to the removal from their mother ion during the laser pulse. The mutual attractive Coulomb potentials have soft cores. All existing charged particles, ions and electrons, are propagated classically exposed to their mutual attraction and repulsion as well as to the coupling with the light pulse. Handling up to about ten electrons per atom implies a total of up to 10^5 particles to be propagated over relative long times (of the order of hundred optical cycles). This is not possible with standard molecular dynamics but requires tree-code techniques [11]. Alternatively, one can start from the particle-in-cell concept to handle clusters of this size [12].

3 Energy spectra of cluster electrons during the laser pulse

In this section we present and interpret the energy spectra of the electrons. An overview of the spectra is given in Fig. 1, the parameters for each panel of figure Fig. 1 are provided in Table 1. Basically, for each pulse length T the peak intensity increases by a factor of 5 from top to bottom (set A to C). For increasing pulse lengths T from left to right the fluency of the pulse remains the same. Hence, from one figure to the next the peak intensity decreases by a factor of 2 since the pulse length increases by a factor of 2. All figures show distributions of total energies of the electrons on the y -axis ranging from -10 keV to $+5$ keV with the total energy of electron i at position \mathbf{r}_i with momentum \mathbf{p}_i defined as

$$E_i = \frac{\mathbf{p}_i^2}{2} - \sum_a^{\text{ions}} \frac{q_a}{|\mathbf{r}_a - \mathbf{r}_i|} + \sum_{j(\neq i)}^{\text{electrons}} \frac{1}{|\mathbf{r}_j - \mathbf{r}_i|} \quad (2)$$

with \mathbf{r}_a and q_a the position and the charge of ion a , respectively.

The time evolution of the spectrum is shown from $-T$ to $\max\{+T, 100 \text{ fs}\}$. Of course, the calculation of the dynamics sets in long before $-T$, when the pulse intensity is still negligible. It should be pointed out that Fig. 1 contains for each plot and at each time the energies of up to 10^5 electrons. Just the generation of such a plot in a reasonable time requires to use the tree-code information.

Table 1. Laser pulse parameters for the 15 plots in Fig. 1. The peak intensity I given in units of 10^{15} W/cm^2 and the pulse length T in fs enters Eq. (1). Furthermore, the quiver amplitude $x_\omega = \sqrt{I}/\omega^2$ is given in Å and the ponderomotive energy $U_p = I/4\omega^2$ in units of eV, whereby $\omega = 0.058$ a.u., the laser frequency corresponding to 780 nm wavelength.

T		25	50	100	200	400
set A	I	3.2	1.6	0.8	0.4	0.2
	x_ω	46.7	33.1	23.4	16.5	11.7
	U_p	181	90.7	45.4	22.7	11.3
set B	I	16	8	4	2	1
	x_ω	105	73.9	52.3	37.0	26.1
	U_p	907	454	227	113	56.7
set C	I	80	40	20	10	5
	x_ω	234	165	117	82.6	58.4
	U_p	4536	2268	1134	567	284

3.1 Common features in all spectra

A first orientation in the plots reveals that the lowest electron energies go always through a minimum after the laser pulse has reached its maximum intensity. The minimum assumes quite different values, for the parameters in Fig. 1 roughly between -2 and -15 keV. The negative electron energies are due to the positive background charge $Q_t = \sum_a q_a$ of the cluster which is a direct consequence of ionized electrons which have left the cluster. They appear at positive energies in the plots. As stronger the cluster is ionized as deeper the remaining electrons are bound by the back ground charge. Upon explosion of the ions the background charge spreads out and consequently, the energy of the trapped electrons decreases for longer times. Evident are two preferred energy regions (with high intensities) for the electrons: Ionized electrons have excess energies close to $E = 0$. The trapped electrons prefer energies close to the lowest possible values.

3.2 General trends as a function of peak intensity: The role of the quiver amplitude

The population of the two preferred regions is most prominent in the lower left corner of Fig. 1, i.e., for maximum peak intensity. For minimum peak intensity (upper right corner) the opposite trend can be identified: A substantial number of electrons fills the area (of negative energy) between the two preferred regions. If one compares the equilibrium size of the cluster given by the radius $R_0 = 50$ Å with the quiver amplitude of an electron in the laser field $x_\omega = \sqrt{I}/\omega^2$, listed in Table 1, the reason for this trend becomes obvious: For largest intensities (lower left corner) $x_\omega > R_0$ and the ionized electrons are driven far outside the cluster. The opposite is true for low intensities (upper right corner) with the lowest intensities where despite quivering in the laser field the electrons remain well inside the cluster, leading to a distribution of negative electron energies due to the attractive background charge.

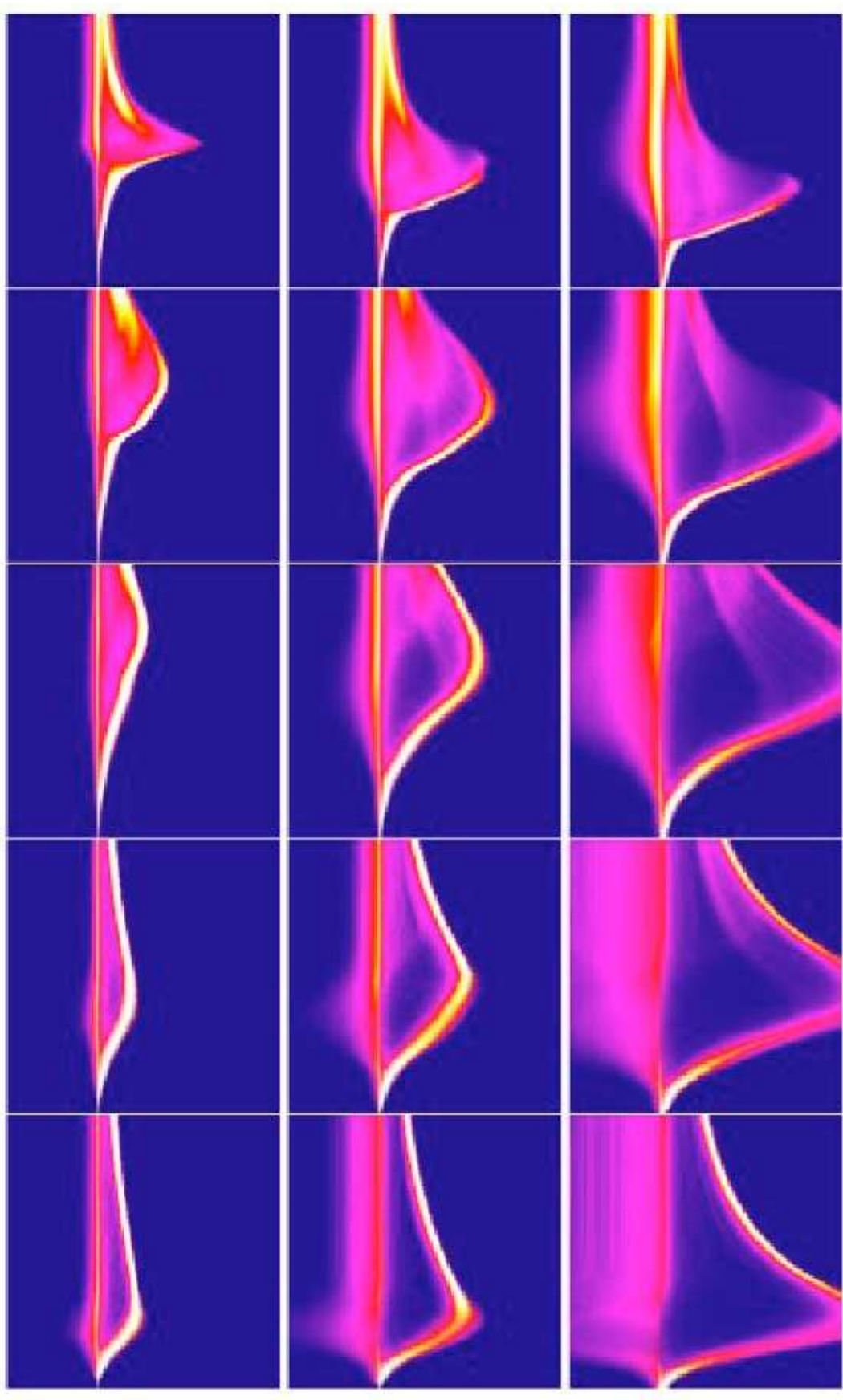


Fig. 1. Energy distribution of electrons according to Eq. (2) under illumination of a Xe_{9093} cluster with laser pulses of different pulse length T and peak intensity I as detailed in Table 1. The pulse shape is given in Eq. (1). The visible area has range of energy on the y -axis between -10 keV and $+5$ keV, and a range of time on the x -axis between $-T$ and $\max\{T, 100$ fs $\}$.

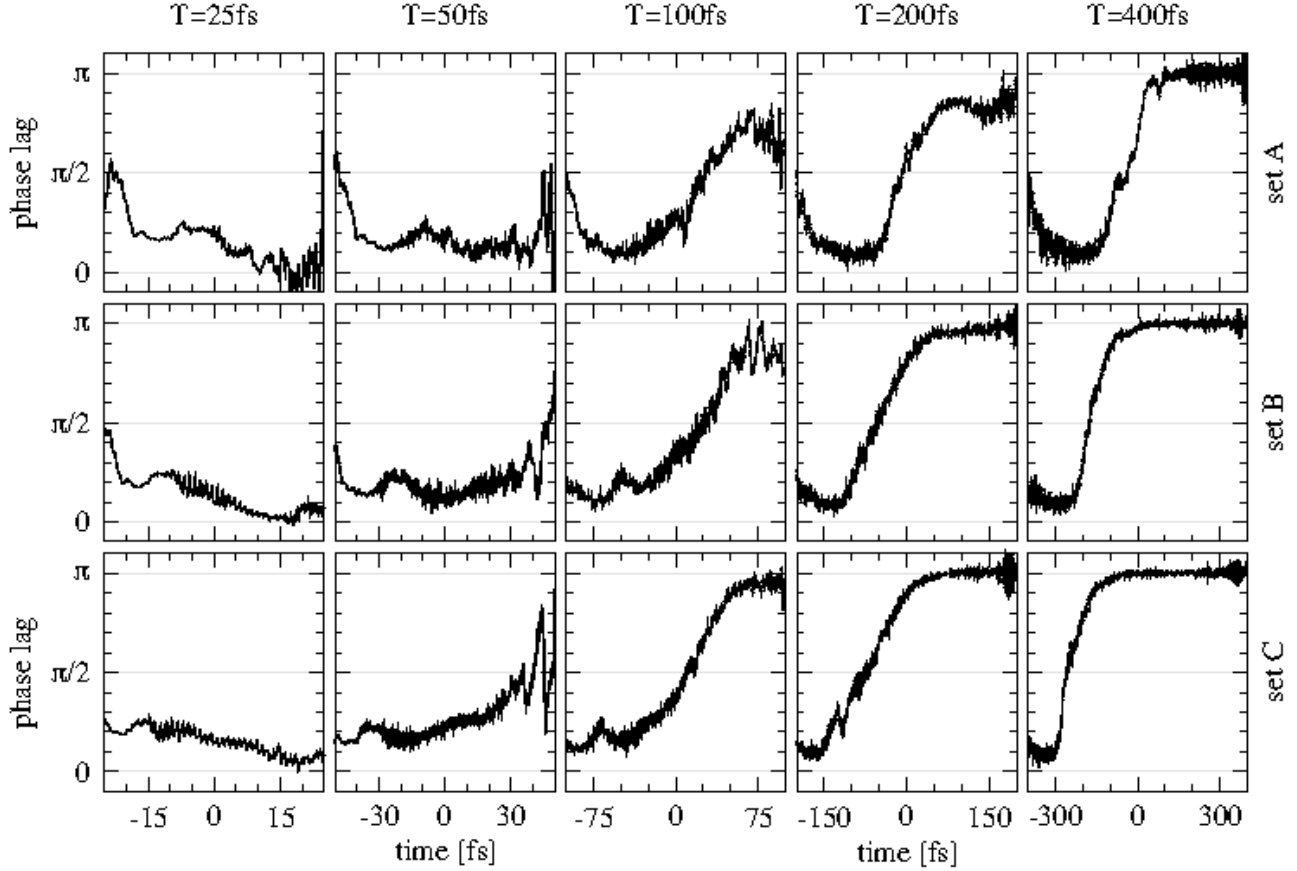


Fig. 2. Phase difference between laser cycle and periodic response of electrons inside the cluster volume for the same laser pulse parameters as shown in Fig. 1.

3.3 The trace of escaping single ions

In the panels corresponding to large pulse lengths and high peak intensity (lower right corner of Fig. 1) one sees individual lines of electron energies above the energy minimum and converging to each other for longer times. These lines are energies of electron being trapped in excited orbits around a single ion due to rising interatomic barriers when the cluster expands. Hence, large pulse lengths are necessary for this feature. It also occurs in the upper right corner of Fig. 1 (i.e., for lower intensities) but it is masked there by other electrons with similar energies. They cannot leave the cluster since the laser intensity is too low.

3.4 Atomic versus cluster effects

Very short pulses in small clusters explore primarily atomic properties of the atoms and ions within the cluster since there is not enough time for a cooperative response of the cluster as a whole, e.g. by expansion or thermalized collective electron motion. Large clusters, however, develop upon the first atomic field ionization for each atom a substantial positive background charge (in our case roughly

$Q = +10^4$ for single ionization of the atoms). The main mechanism for further ionization is therefore the escape from the potential generated by the background charge. It can be modelled by assuming a homogeneously charged sphere with total charge Q_t and (cluster) radius R_t , which leads to the potential

$$V_t(r) = \begin{cases} -Q_t(3R_t^2 - r^2)/(2R_t^3) & \text{if } r \leq R_t \\ -Q_t/r & \text{if } r \geq R_t, \end{cases} \quad (3)$$

where quantities with subscript t are weakly time dependent. All electrons in this potential can leave the cluster if the height of the potential barrier at maximum field strength within a laser period is lower or equal to the potential minimum. This happens at the field strength F_t that shifts the potential minimum from $r = 0$ to the cluster surface $r = R_t$, i.e. $[dV_t(r)/dr]_{R_t} = F_t$. From this the maximum charging of the cluster can be estimated to be

$$Q_t = R_t^2 F_t. \quad (4)$$

The depth of the minima in the energy of the electrons in Fig. 1 indicates directly the charging of the cluster. Hence, if Eq. (4) is true the depth and the early charging process in time should agree if the energy (y -axis) in the panels is

scaled by F_t . Indeed, for the three panels A–C belonging to $T = 25$ fs and $T = 50$ fs the temporal development of the electronic energy until the minimum is reached agrees very well after scaling (not shown). The considerations apply as long as the cluster has not expanded yet, i.e., $R_t \approx R_0$. For longer times the cluster expands and the scaling does not apply.

3.5 Resonant energy absorption through collective electron motion

If the pulse is long enough to allow for an expansion of the cluster during the illumination by laser light resonant absorption becomes possible. The mechanism behind resonant absorption in a cluster of the present size is the match between the frequency of collective electron motion within the cluster and the laser frequency. This leads to a characteristic phase lag of $\pi/2$ between the oscillation of the laser amplitude and the electronic response [6]. If one compares Fig. 2 with Fig. 1 one sees that resonant absorption goes hand in gloves with a sharp decrease of the minimum electron energy (i.e. a fast charging of the cluster). This is clearly visible in all panels for $T = 400$ fs and in panel A for $T = 200$ fs. If the resonance occurs during the fall of the laser envelope ($t > 0$) it cannot be directly recognized in the electron energy (compare Fig. 1 with Fig. 2).

3.6 Fine structure on the scale of the optical cycle

Finally, we would like to draw attention to a peculiar behavior in the periodic response of continuum electrons and bound electrons to the driving laser. Most intensity of such electrons can be found close to $E = 0$ and close to the minimum of the electron energies, respectively. Firstly one sees that the spots of high electron density occur for bound and continuum electrons with a phase difference of half a period, cf. Fig. 3. Secondly, and may be even more puzzling on a first glance, the energy distribution of the electrons seems to “breeze”, with a narrow distribution at zero field and a wide distribution at maximum field for the bound electrons and exactly the opposite, although less pronounced, for the continuum electrons, cf. Fig. 4.

The behavior of the continuum electrons ($E_i > 0$) in Fig. 3 is easily understood. They have a certain spread of drift velocities $\bar{\mathbf{p}}_i$ or momenta as a result of the energy absorption and the individual electron has an energy of $E_i = (\bar{\mathbf{p}}_i + \mathbf{A}(t))^2/2$ with $\mathbf{A}(t) = \hat{\mathbf{z}} \int^t d\tau F(\tau) \approx \hat{\mathbf{z}} F_t/\omega \sin \omega t = \hat{\mathbf{z}} F_t/\omega \cos(\omega t - \pi/2)$. In other words, since these electrons oscillate with a phase lag of π the velocity or the momentum has a phase lag of $\pi/2$. Hence, the spread of the $\bar{\mathbf{p}}_i$ is amplified due to the squaring in the energy E_i at zero field, as can be seen from the peaks between the white lines in the upper part of Fig. 3 and from the corresponding distribution of energies $E_i > 0$ in Fig. 4 (black curve).

The energies E_i of the bound electrons ($E_i < 0$ in Fig. 3) show a similar spreading phenomenon, however

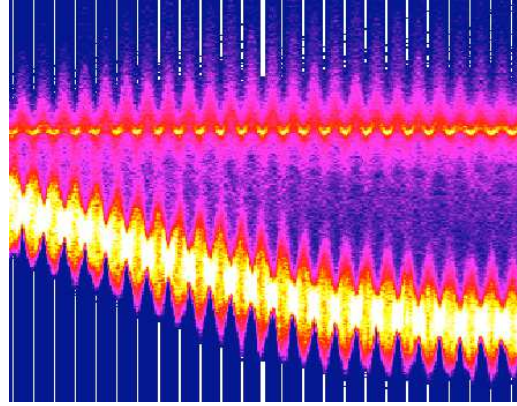


Fig. 3. Magnification of the electron spectrum of series A at $T = 50$ fs from Fig. 1. The white lines indicate times of maximum field strength, the thick white line indicates the time of the cut through the spectrum shown in Fig. 4.

with maximum spread at maximum field. This can be understood if one takes into consideration that the many electrons in the cluster are an interacting system of charges which reacts very fast to forces, trying to reach an equilibrium position and thereby maintaining the spatial distribution in the cluster. In a first approximation it can be assumed to be incompressible. This distribution is driven by the laser and has a vanishing phase lag since the eigenfrequency $\Omega_t^2 = Q_t/R_t^3$ of the cluster potential Eq. (3) is larger than the laser frequency ω . Hence, the total energy E_i of electron i is approximately

$$\begin{aligned} E_i &\approx \frac{\mathbf{p}_i^2}{2} - \frac{3Q_t}{2R_t} + \frac{\Omega_t^2}{2} \left(\bar{\mathbf{r}}_i + \frac{\mathbf{F}(t)}{\Omega_t^2} \right)^2 + \sum_{j(\neq i)} \frac{1}{|\mathbf{r}_j - \mathbf{r}_i|} \\ &\approx \frac{\mathbf{p}_i^2}{2} + V_i(r_i) + \bar{\mathbf{r}}_i \mathbf{F}(t) + \sum_{j(\neq i)} \frac{1}{|\mathbf{r}_j - \mathbf{r}_i|}. \end{aligned} \quad (5)$$

To arrive at Eq. (5) from Eq. (2) we, firstly, replaced the ionic potential by the cluster potential (3) and, secondly, neglected the small term quadratic in \mathbf{F} . From Eq. (5) it becomes clear that by monitoring E_i we see essentially the coupling to the field, i.e.,

$$E_i = E_t^{(i)} + \bar{\mathbf{r}}_i \mathbf{F}(t) \quad (6)$$

where $E_t^{(i)}$ is the energy which varies slowly in time. The spread in E_i results from the different positions $\bar{\mathbf{r}}_i$ of the electrons within the cluster, $|\bar{\mathbf{r}}_i| \leq R_t$. Indeed, the spread is amplified through the laser field amplitude for maximum field while the electron energy is focused to a small range at zero field, in accordance with the observation in Fig. 3 or more clearly in Fig. 4.

4 Summary

We have analyzed the time-dependent distribution of electron energies resulting from the illumination of a large

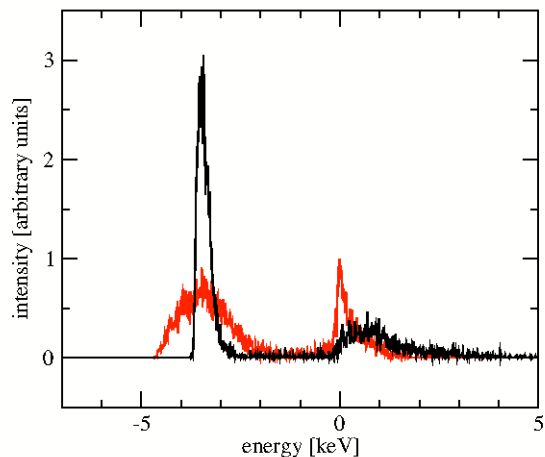


Fig. 4. Cut through the electron energy spectrum of series A at 50 fs in the optical cycle around maximum laser intensity I (time $t = 0$) indicated by a thick white line in Fig. 3. The black curve is for almost vanishing field strength, the red (grey) curve for the maximal field strength within the optical cycle.

cluster containing about 10^4 Xenon atoms with a short intense laser pulse at 780 nm wavelength. The spectrum shows a rich structure on the time scale of the optical laser period with many interesting details which would be worthwhile to probe in the future using attosecond techniques. This might be even possible in the near future since extended systems like a cluster show interesting electron dynamics on the 100 attosecond time scale while more tightly bound electrons in atoms or ions are too fast for direct probing with pulses of 10–100 attosecond length.

Moreover, for now we do not have detailed knowledge about time resolved electron motion in clusters and such experiments would also reveal if our way of describing this dynamics theoretically is adequate.

References

1. M. Hentschel, R. Kienberger, Ch. Spielmann, G. A. Reider, N. Milosevic, T. Brabec, P.B. Corkum, U. Heinzmann, M. Drescher, and F. Krausz, *Nature* **414**, 509 (2001).
2. H. Niikura, F. Légaré, R. Hasbani, A. D. Bandrauk, M. Yu Ivanov, D. M. Villeneuve, and P. B. Corkum, *Nature* **417**, 917 (2002).
3. J. Itatani, J. Levesque, D. Zeidler, H. Niikura, H. Pépin, J. C. Kieffer, P. B. Corkum, and D. M. Villeneuve, *Nature* **432**, 867 (2004).
4. L. Köller, M. Schumacher, J. Köhn, S. Teuber, J. Tiggesbäumker, and K. H. Meiwes-Broer, *Phys. Rev. Lett.* **82**, 3786 (1999). T. Döppner, Th. Fennel, Th. Diederich, J. Tiggesbäumker, and K. H. Meiwes-Broer, *Phys. Rev. Lett.* **94**, 013401 (2005).
5. Ch. Siedschlag and J. M. Rost, *Phys. Rev. Lett.* **89**, 173401 (2002).
6. U. Saalmann and J. M. Rost, *Phys. Rev. Lett.* **91**, 223401 (2003).
7. S.V. Fomichev, S.V. Popruzhenko, D.F. Zaretsky, and W. Becker, *J. Phys. B* **36**, 3817 (2003).

8. H. Wabnitz, L. Bittner, A. R. B. de Castro, R. Döhrmann, P. Gürtler, T. Laarmann, W. Laasch, J. Schulz, A. Swiderski, K. von Haeften, T. Möller, B. Faatz, A. Fateev, J. Feldhaus, Ch. Gerth, U. Hahn, E. Saldin, E. Schneidmiller, K. Sytchev, K. Tiedtke, R. Treusch, and M. Yurkov, *Nature (London)* **420**, 482 (2002).
9. R. Santra and C. H. Greene, *Phys. Rev. Lett.* **91**, 233401 (2003).
10. Ch. Siedschlag and J. M. Rost, *Phys. Rev. Lett.* **93**, 043402 (2004).
11. S. Pfalzner and P. Gibbon, *Many-body tree methods in physics*. Cambridge University Press 1996.
12. C. Jungreuthmayer, M. Geissler, J. Zanghellini, and T. Brabec, *Phys. Rev. Lett.* **92**, 133401 (2004).